land

MDPI

Article

Hydrological Regime, Provenance, and Impacts on Cultural Development at Changsha Kiln Archaeological Site since 1300 a, Lower Xiangjiang River, China

Aipeng Guo [1], Longjiang Mao [2,*], Siwei Shan [3], Xingguo Zhang [4] and Duowen Mo [5]

1 Research Base for Scientific Cognition and Protection of Culture Heritage, Nanjing University of Information Science &Technology, Nanjing 210044, China; 20201129002@nuist.edu.cn
2 School of Marine Science, Nanjing University of Information Science and Technology, Nanjing 210044, China
3 Department of Archaeology, School of History, Wuhan University, Wuhan 430032, China; swshan@whu.edu.cn
4 Archaeology Institute of Hunan Province, Changsha 410008, China; gap18551543661@163.com
5 College of Urban and Environmental Sciences, Peking University, Beijing 100871, China; dmo@urban.pku.edu.cn
* Correspondence: mlj1214@nuist.edu.cn

Abstract: Changsha kilns were exported to more than 20 countries and regions and were an essential part of the culture in the central Yangtze River during the late Holocene. Reconstructing the hydrological landform and sedimentary history of its surrounding areas (Shizhu) is significant for further constraining any links between regional paleoenvironmental change and the human−land relationship in the lager river valley. To examine paleo−hydrological and provenance evolution, the rare earth element (REE) and trace element ratio from the Shizhuping (SZP) section were analyzed. The SZP section records the paleo−hydrological evolution over 1300 years: river network cutting plain landscape—Shizhu Lake—river floodplain—Shizhu Lake reformation—Shizhu flat. This section was labeled as stages IV to I, respectively. The deposition of stages IV was wind and dust accumulation during the Last Glacial. The provenance of stages III (1288–1094 a.BP) was wasted from the ceramic production process. The layer of stage II (1094–380 a.BP) was in two parts. In stage II−2 (1094–890 a.BP), provenance was dominated by granite. Sedimentary rocks became the source of stage II−1 (890–380 a.BP). In stages I (380 a.BP–), the primary material sources were anthropogenic bedding and weathering erosion deposits around the slope. During the Medieval Warm Period, the climate was warm and humid, and the rising water level of the Xiangjiang River led to the emergence of lakes in the Shizhu area. The migration of northern China into Changsha kiln brought new technology and labor. In the late Five Dynasties, the climate turned dry, and the falling water level of the Xiangjiang River caused Changsha kiln to lose its commercial wharf.

Keywords: rare earth element; trace element; provenance; paleo−hydrological reconstruction; Changsha kiln

check for updates

Citation: Guo, A.; Mao, L.; Shan, S.; Zhang, X.; Mo, D. Hydrological Regime, Provenance, and Impacts on Cultural Development at Changsha Kiln Archaeological Site since 1300 a, Lower Xiangjiang River, China. *Land* **2022**, *11*, 789. https://doi.org/10.3390/land11060789

Academic Editors: Minmin Ma, Xianyong Cao and Guanghui Dong

Received: 8 April 2022
Accepted: 25 May 2022
Published: 27 May 2022

1. Introduction

The evolution of climate, hydrology, and geomorphic environment is closely linked to human civilizations [1,2]. However, in large river basins and deltas, the interplay of climate systems and regional hydrological dynamics complicates the process of cultural responses to environmental change [3–5]. Early agricultural societies during the late Holocene relied on a favorable and stable environment and had difficulty adapting to the abrupt climatic deterioration [6]. For instance, Holocene event 3 had a significant influence worldwide at around 4200 a. BP [7]. The decrease in river flow and lake degradation caused by the arid climate is coherent with the termination of regional cultural processes in the Indus [8,9], Mississippi [10,11], and Yangtze River valleys [12,13]. Subsequently, the impact of human activities on the environment and climate fluctuations gradually increased in the Medieval Warm Period and Little Ice Age [14,15]. Given the relationship of late Holocene people to hydrology and climate, the reconstruction of the paleoenvironment is critical for comprehending human communities [16,17].

The Yangtze River Vally is the third−largest in the world, and its regional climate is controlled by the dual impacts of the East Asian monsoon and the Southwest monsoon [18]. The Xiangjiang River basin in Central Yangtze River is an early center of rice agriculture and pottery development [13,19]. The impact of relatively noticeable shifts in the East Asian monsoon on temperature and precipitation in the Central Yangtze River region makes the Xiangjiang River basin an ideal zone for paleoenvironmental studies [20–22]. Between the 9th–10th century AD, the Changsha kiln and Yue kiln in the Yangtze River Valley marked the earliest mass production centers of ceramics in China [23]. The Silk Road had both land and water routes, and the ceramic trade during the Tang Dynasty relied more on the water route. The Yangtze River was part of the water route connecting China with other countries [23,24]. Merchants of the Changsha kilns entered the Yangtze River from the Xiangjiang River and sold their goods worldwide through the Maritime Silk Road [24]. In the 9th century, Changsha kiln products were exported to more than 20 countries, reaching as far as Tanzania in eastern Africa [23]. The Changsha kiln was notable chiefly for its colorful porcelain, which flourished in the Shizhu area in Changsha [25,26]. The dense river network and the rich porcelain soil resources laid the foundation for developing the ceramic industry [27]. The Shizhu area was a low−lying estuary region on the Xiangjiang River. It was highly vulnerable to even minor changes in water level, environmental events, and human activity, including flood and embankment construction [21,28,29]. Therefore, the development of the Changsha kiln is very dependent on a local stable hydrological environment. Previous studies have argued that human activities in the Shizhu area may be tightly associated with vegetation dynamics, climate [21], and fire patterns [29]. Others have discussed ceramic technology, such as glaze composition and rare earth element characteristics of ceramics [26,30]. Systematic investigations of the paleo−hydrological evolution around the Changsha kiln are scarce. The Changsha kiln, which had a massive scale in the Indian Ocean trade [23], disappeared at the end of the Five Dynasties (906–907 AD) [28]. Studying the environmental background of its prosperity and decline is significant for understanding the relations between man and land in the Xiangjiang River Valley during the Late Holocene.

The rare earth elements (REEs) refer to a set of metallic elements with homogeneous electronic structure and chemical properties, including lanthanides, scandium (Sc), and yttrium (Y) [31,32]. The ionic state of REEs mainly exists in the trivalent state, except for Ce and Eu [33]. Both δCe and δEu are essential REE parameters related to provenance and environment [34]. In general, REEs are characterized by weak mobility and negligible elemental fractionation during the weathering, transport, deposition, and diagenesis of source rocks [35,36]. Due to their conservative characteristic, REEs are frequently applied as reliable source tracers in the evolution of river or marine provenance [37–39], applied to reflect water−rock interactions [40,41], source area characteristics [42,43], human disturbances [34,44,45]. Trace elements have multiple valence states and can exhibit different geochemical behavior under varying redox conditions, so they can be employed to reconstruct the water oxidation−reduction environment [46]. Redox−sensitive elements, such as Mo, U, V, Ni, and Cr, can reflect different enrichment degrees in redox environments [15,47,48]. Therefore, trace element ratios have been widely adopted to record the changes in palaeo−redox conditions in the river and marine sediments [41,49,50]. The inquiry of trace elements in sediments from the Changsha kiln presented herein provided a critical data point for the study of paleo−hydrological and provenance changes in the Xiangjiang River. It offered a novel perspective on the natural and social environment research in the Changsha kiln.

This study made considerable efforts to analyze trace elements and their characteristics in the Shizhuping (SZP) section in Changsha kiln near the Shizhu area and combined element ratios and archaeological data. The main issues addressed in this paper are to (1) reconstruct the paleo−hydrological dynamics of Xiangjiang River; (2) identify the provenance changes of the SZP sediments; (3) discuss the relationship between paleo−environment change and human activity in the Xiangjiang River.

2. Geographical Setting around Changsha Kiln Site

The SZP section (28°25′092″ N, 112°49′35.7″ E, elevation 24 m above sea level) is about 50 m away from the Xiangjiang River, within the boundaries of the Changsha kiln archaeological site (Figure 1). The mainstream of the Xiangjiang River is 844 km long, with a basin area of nearly 94,660 km^2. More than 1300 tributaries along the way converged here, and the annual average runoff is 72.2 billion cubic meters [51]. In terms of the flow direction, Qi water, Zhen water, trickle water, Lian water, and Wei water come from the west into the mainstream; Xiaoshui Water, Chonglingshui water, Leishui water, Moshui water, Lushui water, and Liuyang River come from the east into the mainstream [52]. These tributaries are located in the upper reaches of the kiln area and are potential source areas for provenance. The average annual temperature is about 17 °C, and the annual precipitation is 1200–1700 mm, with 60–70% of the precipitation occurring during the flood season [20].

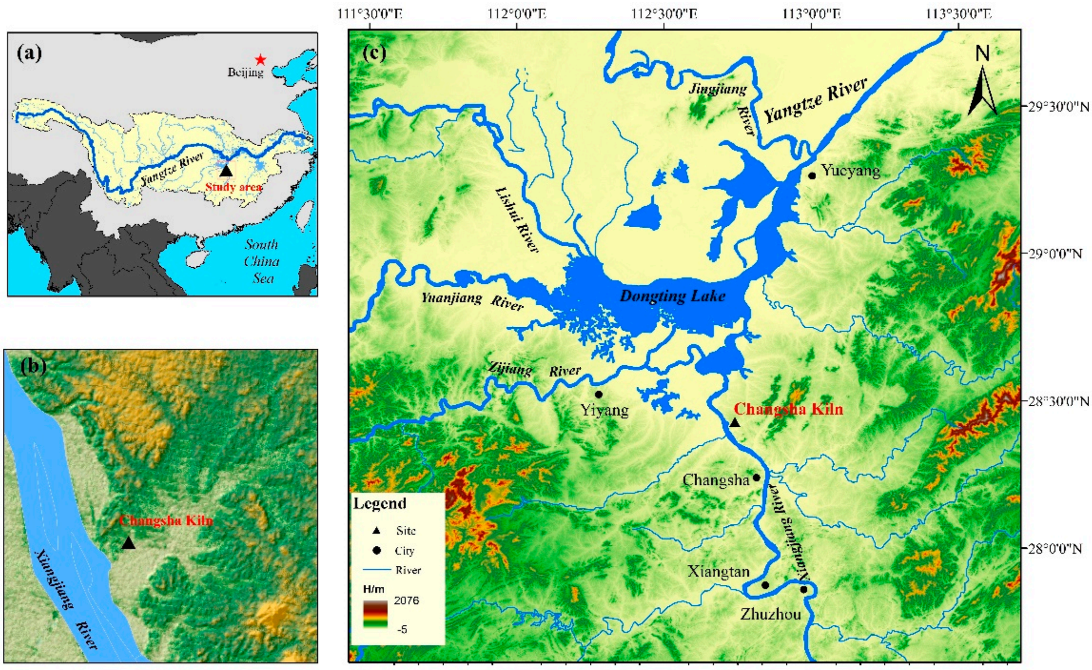

Figure 1. (**a**): Location of the study area in the Yangtze River Vally, (**b**): Geomorphological features of the Shizhu area, (**c**): An overview map of the lower reaches of the Xiangjiang River, where the Changsha kiln is marked by the black triangle.

The Xiangjiang River is the main river in Changsha, Hunan province. The Xiangjiang River basin is tectonically complex on the Yangzi Platform and the South China Fold [53], with stratigraphic rocks: pre−earthquake sandstones and slates, Paleozoic carbonates, Middle Cenozoic sandstones, Indochinese and Yanshanian granites (upstream areas), and Quaternary sediments exposed [54]. The upper reaches of the basin (south of Lingling) are dominated by Devonian sand, shale, and Devonian Carboniferous limestone. The mid−lower reaches (Lingling to Zhuzhou) are Mesozoic and Cenozoic purple sandstone. The soils are mainly derived from shale, sandstone, purple sandstone, and laterite [54,55].

3. Materials and Methods

3.1. Stratigraphy and Sampling

The SZP section is a specially excavated parallel section on the river terrace of the east bank of the Xiangjiang River. The section was 320 m long, and the bottom unseen. Samples were taken from intervals at 2 cm or 10 cm, and a total of 99 samples were obtained, numbered SZP001–099. The cultural layer was 260–290 cm, and many pottery blocks and pieces were unearthed, dating to about the middle and late Tang Dynasty. Stratigraphic delineation is based on the comprehensive observation of sediment profile color, structure, and cultural deposit. The profile descriptions are presented in Table 1.

Table 1. Description of the SZP section.

Depth (cm)	Pedological Description
0–70	Yellowish gray clay; Black patches and cutans, red piece, pale gray pebble gravel, and abundant bio−pores, 5–10 cm, fragments of gray pottery
70–80	Yellowish gray clay; Abundant red iron−manganese cutans
80–145	Pale gray mud; Reddish yellow cutans, bio−pores
145–215	Pale yellow Silty clay
215–230	Yellowish gray clay
230–260	Gray mud; Abundant pottery debris, charcoal
260–290	Cultural layer during the middle−late Tang dynasty; Abundant ceramic pieces, Braised clay
290–310	Yellowish gray clay; some Braised clay, abundant charcoal, 5–10 cm thickness
>310	Pale yellow raw soil

3.2. Geochemical Element Analyses

All samples were naturally dried in the laboratory. 5 g of each sample was ground and passed through a sieve with a diameter of 75 μm. The samples were dried in an oven at 105 °C. After drying, 25 mg of the sample was weighed and placed in a homemade high−pressure sealed dissolution device. Concrete steps are as follows: (1) Add 0.5 mL of concentrated HF and evaporate to remove some Si, then add 1 mL of concentrated HF and 0.5 mL of concentrated HNO_3 to dissolve at 190 °C and evaporate to a wet salt state. (2) Add 1 mL of HNO_3 and evaporate to a wet salt to remove excess HF. (3) Add 5 mL 30% (V/V) HNO_3 and heat it sealed at 140 °C for 4 h. (4) After cooling, 1 mL 500 ng/mL Rh internal standard solution was added and diluted to 50mL to reduce matrix effect and instrument drift.

A total of 14 REEs (La, Ce, Pr, Nd, Pm, Sm, Eu, Gd, Dy, Er, Yb, Ho, Tb, Tm, Lu.) and some trace elements(Rb, Sr, V, Ni) were measured, and the errors were less than ±10% when the results were compared with those of the standard samples. After pretreatment, the REE contents were measured through high−resolution inductively coupled plasma−mass spectrometry (HR−ICPMS) [56]. The experiments were completed at the State Key Laboratory for Mineral Deposits Research of Nanjing University. The concentrations of light rare earth elements (LREE) were the sum of La−Eu, and heavy rare earth elements (HREE) were the sum of Gd−Lu. Concentrations of rare earth elements (ΣREE) were the sum of La−Lu. The REE characteristic parameters (ΣREE, δCe, δEu, LREE/HREE, $(La/Sm)_N$, $(La/Yb)_N$, $(Sm/Nd)_N$, $(Gd/Yb)_N$) were selected to explore the geochemical characteristics of REEs. Subscript N indicated the normalized abundance with chondrites [57]. The δCe and δEu values, which represent the degree of Ce and Eu anomalies, were calculated using Equations (1) and (2) [58]. δCe, V/(V +Ni), and Ce/La ratios were selected as the main paleo−redox proxies [59,60]. Rb/Sr and Sr were employed as proxies to infer the paleoenvironment [61,62]. The La/Yb−∑REE diagram was used to determine the type of parent rocks in the source region [63]. Correlations were analyzed using Pearson's correlation coefficient(r). The Statistical Package for the Social Sciences was used for the statistical analyses (SPSS, version 26).

$$\delta Ce = \frac{Ce_N}{(La_N \times Pr_N)^{0.5}} \quad (1)$$

$$\delta Eu = \frac{Eu_N}{(Sm_N \times Gd_N)^{0.5}} \quad (2)$$

3.3. Chronology

All samples were measured at the AMS14C/OSL (Calibrated with CALIB 7.01) Laboratory of the Peking University in China. Four 1 m steel tubes were driven into the profile, and the tubes were removed and wrapped in tinfoil after 24 h. Three OSL and one AMS^{14}C sample were collected at 139–141 cm, 149–151 cm, 94–96 cm, and 290–292 cm, respectively (Table 2). In addition, the pottery fragments unearthed at 260–290 cm were identified as cultural relics from the middle and late Tang Dynasty (1240–1160 a.BP). Based on those chronologies, an age−depth model was established to interpret the last 1300 years of the sedimentary history of the Xiangjiang river basin. The model was built and successfully used in Tan's publication [29].

Table 2. AMS^{14}C/OSL age data in the SZP profile (date from Tan's publication) [29].

Sample	Depth (cm)	AMS^{14}C/OSL Date
AB120171	94–96	451 ± 32
AB120172	139–141	879 ± 65
AB120173	149–151	1182 ± 85
BA120171(AMS^{14}C)	290–292	1320 ± 30

3.4. Grain Size

The grain size experiment was carried out in the laboratory of marine sedimentology, Nanjing University of Information Science and Technology. Sediment samples received treatments in test tubes with approximately 5 mL 3 M hydrochloric acid (HCl) and 15 mL 3% H_2O_2 to eliminate carbonates and organic matter. The sample went through a 2 mm sieve. After ultrasonic oscillation, the particles were dispersed entirely. The particle size was measured by a laser particle size analyzer (Malvern 2000, range: 0.02–2000 µm, resolution: 0.01 φ). The relative error of repeated measurements is ±3%.

4. Results

4.1. Dating Results

An age−depth curve was established with the sediment dating and ceramic archaeological results from the remains (Figure 2). The middle of the paleosol (94–96 cm) under the cushion soil was OSL age dated 451 ± 32 a.BP. The pale yellow silty clay (139–141 cm) and yellowish gray clay (149–151 cm) in the middle of the profile were OSL ages dated to 879 ± 65 a.BP and 1182 ± 85 a.BP, respectively. The cultural layer at the bottom was AMS^{14}C ages dated to 1320 ± 30 a.BP. Overall, the ages indicated a continuous sedimentary history of 1300 a.BP and increased with depth.

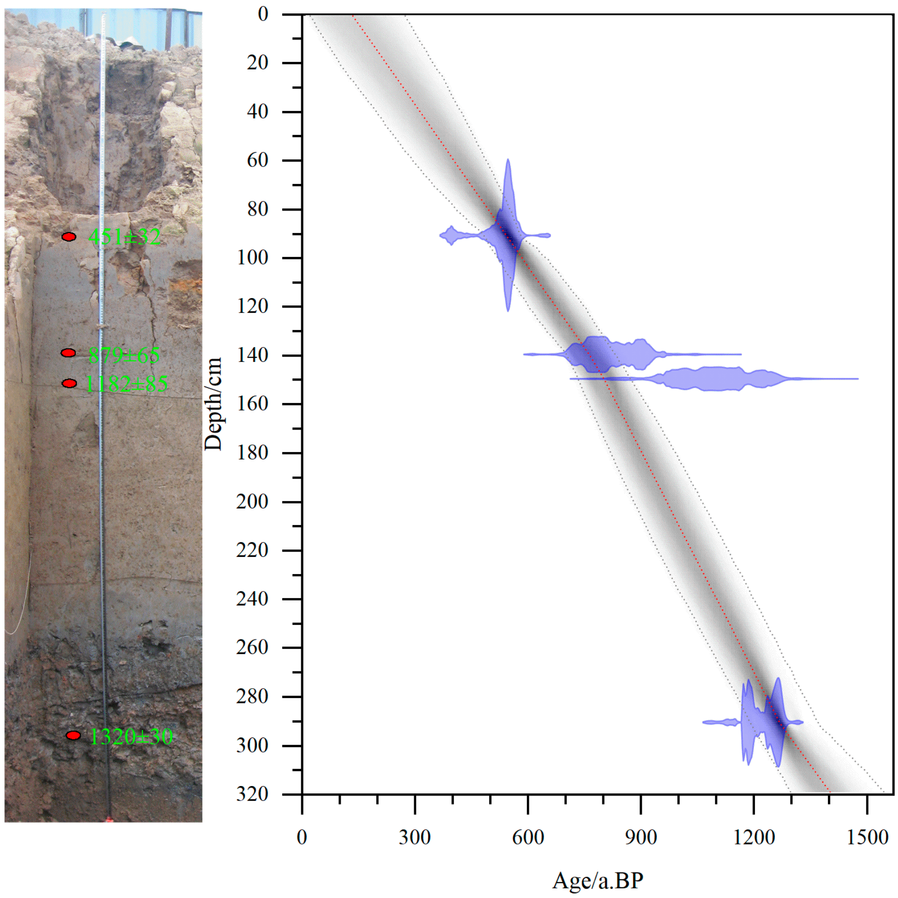

Figure 2. Stratigraphy and age−depth model of the SZP section, adapted from Tan's result [29].

4.2. Contents and Trends of REEs in SZP Profile

The average concentration of ΣREE is 235.55 mg·kg^{-1} in the SZP section, fluctuating from 203.33 to 258.07 mg·kg^{-1}, much higher than the average REE content of the upper crust (146 mg·kg^{-1}) [64] and that of the local soil background [65] (151 mg·kg^{-1}). REEs concentrations tend to be lower with increasing atomic number adhering to Oddo−Harkins principle [66]: Ce > La > Nd > Pr > Sm > Gd > Dy > Er > Yb > Eu > Ho > Tb > Lu > Tm.

The vertical distribution of REEs was measured to quantify and obtain a better understanding of the distribution and trends of REEs in the profile (Figure 3). The trends in each REE content distribution are distinguishable from the bottom to the surface layer. The section can be discussed in four stages based on the direction of changes in the ΣREE and the stratigraphic observations. The source soil of stage four is not the red soil widely distributed in southern China but loess. The mean value (236.8 mg·kg^{-1}) of ΣREE in stage IV was close to the XiaShu loess (207.7 mg·kg^{-1}) [67] and the Yangtze River floodplain sediments (233.6 mg·kg^{-1}) [68], and higher than that of the Malan loess (159.2 mg·kg^{-1}) [69] and Kashmir loess (186.5 mg·kg^{-1}) [70]. The ΣREE varied sharply in stage III with frequent high values. If the two lowest values are removed, the average value can reach 241.2 mg·kg^{-1}, reaching its highest point. The maximum value was much higher than the mean value of SZP (235.6 mg·kg^{-1}), and the LREE/HREE ratio (9.4) also reached its highest value. The ΣREE in stage II peaked (256.2 mg·kg^{-1}) and then receded. It decreases again at 145 cm, and after that, the concentration remains stable. The mean value of stage II−1 (240.8 mg·kg^{-1}) is higher than that of stage II−2 (235.7 mg·kg^{-1}), which is higher than the mean value of SZP (235.6 mg·kg^{-1}). The trend of ΣREE was considered stable in stage I. The mean values of ΣREE in the four stages of the analyzed profiles decreased in the following order: stage II−1 > stage IV > stage II−2 > stage I > stage III. The maximum concentration value occurs in stage II−2 (258.1 mg·kg^{-1}), and the minimum concentration value (203.3 mg·kg^{-1}) occurs in stage III (Table 3).

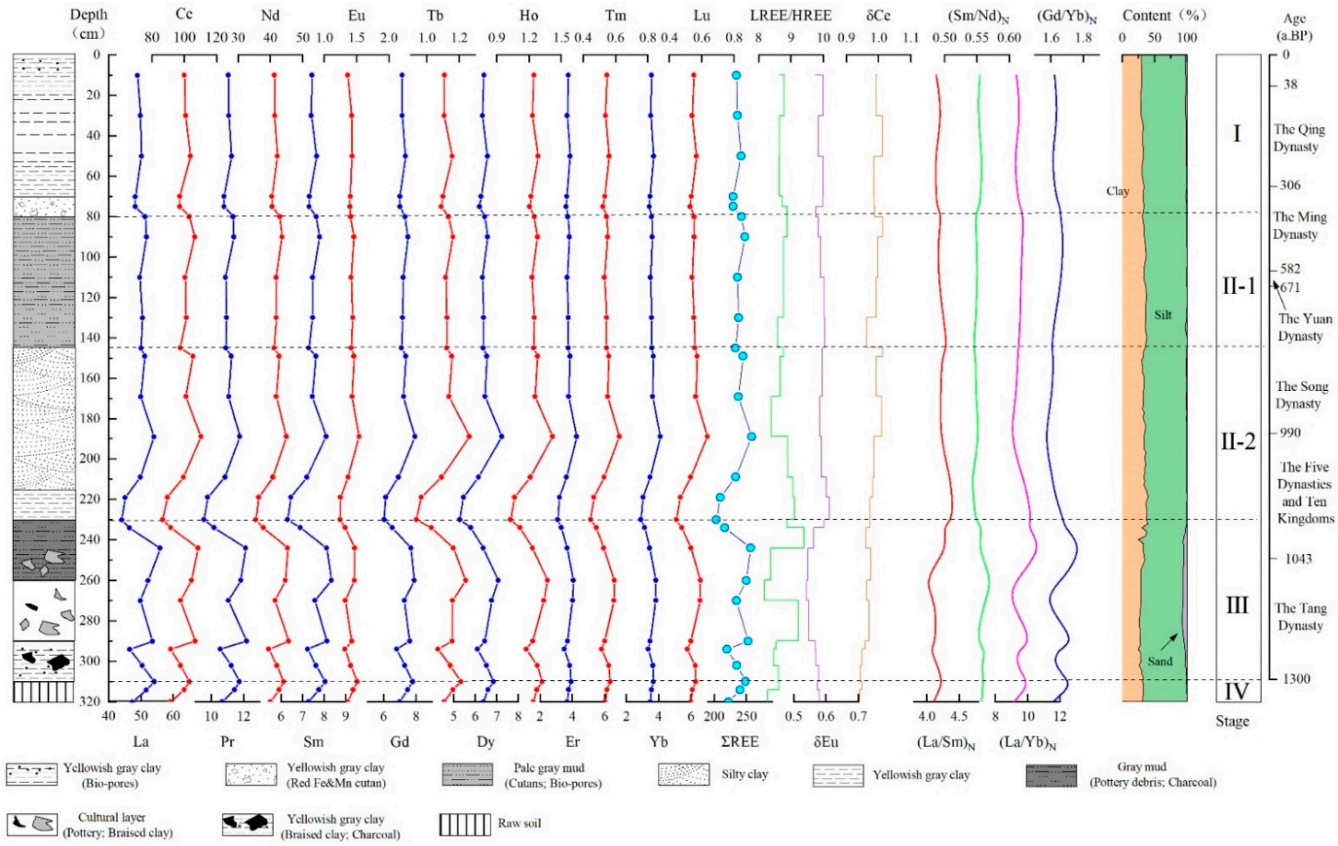

Figure 3. Vertical distribution change of the REEs (mg·kg^{-1}) and Parameter characteristics in the SZP section. The chronological framework of Chinese historical periods was based on the time of the demise of the dynasty (1332 a.BP for the founding of the Tang Dynasty). The profile was divided into four parts, stage I, II, III, and IV based on the variation of the ΣREEs and the lithology. Stage II was analyzed in two parts(II−1, II−2).

Table 3. The REEs concentrations from sediments in the SZP section (mg·kg^{-1}).

Stage		La	Ce	Pr	Nd	Sm	Eu	Gd	Tb	Dy	Ho	Er	Tm	Yb	Lu	ΣREE
I	Max	50.1	103.9	11.3	42.1	7.6	1.4	7.4	1.2	6.6	1.3	3.9	0.6	3.7	0.6	241.5
	Min	48.2	97.1	10.8	40.5	7.3	1.4	7	1.1	6.2	1.2	3.6	0.5	3.4	0.5	229.1
	Mean	49.1	99.8	11	41.1	7.4	1.4	7.1	1.1	6.4	1.2	3.7	0.5	3.5	0.5	234
	[1] SD	0.79	2.51	0.18	0.60	0.13	0.02	0.13	0.02	0.13	0.03	0.09	0.01	0.10	0.01	4.66
II−1	Max	51.7	106.5	11.4	43.6	7.8	1.5	7.5	1.2	6.6	1.3	3.8	0.6	3.6	0.6	247.4
	Min	49.6	100.4	10.9	41.8	7.5	1.4	7.2	1.1	6.3	1.2	3.7	0.5	3.5	0.5	235.7
	Mean	50.8	102.8	11.1	42.5	7.6	1.4	7.3	1.1	6.4	1.3	3.7	0.5	3.6	0.5	240.8
	SD	0.80	2.32	0.23	0.77	0.13	0.02	0.13	0.02	0.09	0.02	0.05	0.01	0.04	0.01	4.53
II−2	Max	54	110.3	11.8	44.9	8.1	1.5	7.9	1.3	7.2	1.4	4.3	0.6	4.1	0.6	258.1
	Min	45.1	89.5	9.8	36.4	6.5	1.3	6.1	1	5.4	1.1	3.2	0.5	3	0.5	209.2
	Mean	50	100.5	10.9	41.3	7.3	1.4	7.1	1.1	6.4	1.2	3.7	0.5	3.6	0.6	235.7
	SD	2.64	6.46	0.60	2.57	0.49	0.09	0.54	0.09	0.53	0.10	0.31	0.05	0.32	0.05	14.72

Table 3. *Cont.*

Stage		La	Ce	Pr	Nd	Sm	Eu	Gd	Tb	Dy	Ho	Er	Tm	Yb	Lu	ΣREE
III	Max	55.9	108.6	12.2	45.6	8.3	1.5	7.9	1.2	7.1	1.4	4.1	0.6	3.8	0.6	256.2
	Min	44	86.6	9.6	35.5	6.3	1.2	6	0.9	5.3	1	3.1	0.4	2.9	0.4	203.3
	Mean	49.8	98.1	11.1	41.5	7.5	1.4	7.1	1.1	6.3	1.2	3.6	0.5	3.4	0.5	233.3
	SD	3.77	7.44	0.89	3.46	0.65	0.08	0.60	0.09	0.53	0.11	0.32	0.05	0.30	0.05	17.81
IV	Max	54.1	103.2	11.7	44.1	8	1.5	7.8	1.2	6.8	1.3	3.9	0.6	3.7	0.6	248.6
	Min	47.3	91.4	10.7	40	7.3	1.4	7	1.1	6.4	1.2	3.7	0.5	3.5	0.5	222
	Mean	51	98.2	11.3	42.3	7.7	1.4	7.4	1.2	6.6	1.3	3.8	0.5	3.6	0.5	236.8
	SD	2.80	4.96	0.45	1.70	0.32	0.06	0.34	0.04	0.19	0.03	0.10	0.01	0.07	0.01	11.06
SZP	Max	55.9	110.3	12.2	45.6	8.3	1.5	7.9	1.3	7.2	1.4	4.3	0.6	4.1	0.6	258.1
	Min	44	86.6	9.6	35.5	6.3	1.2	6	0.9	5.3	1	3.1	0.4	2.9	0.4	203.3
	Mean	50	99.7	11.1	41.6	7.5	1.4	7.2	1.1	6.4	1.2	3.7	0.5	3.5	0.5	235.6
Xiashu		43.7	84	10.4	38.3	7.4	1.5	6.4	0.9	6.3	1.3	3.4	0.5	3.1	0.5	207.7
YR		45.6	106.7	10.9	39.5	7.3	1.6	6.7	1	5.7	1.1	3.3	0.5	3.2	0.5	233.6
Malan		33	66.9	6.7	28.2	5.7	1.1	4.9	0.8	4.6	1	2.7	0.4	2.7	0.4	159.2
Kashmir		40.6	78.3	8.9	33.1	6.8	1.6	5.6	0.8	4.5	1.1	2.5	0.4	2.1	0.3	186.5
Limestone		4.6	7.7	1	3.6	0.7	0.2	0.7	0.1	0.6	0.1	0.4	0.1	0.4	0.1	20.1
Granite		39.7	73.6	8.1	27.7	4.3	0.7	2.8	0.4	1.8	0.3	0.8	0.1	0.6	0.1	160.9
SR		38.7	79.3	9.7	36.3	7.3	1.5	6.9	1.1	6.8	1.4	3.9	0.6	4	0.6	198.1

[1] SD stands for standard deviation.

4.3. Accumulation Pattern

The REEs content of the SZP profile was normalized using the average value of 15 chondrites proposed by Boynton (1984) [57], and the distribution pattern was obtained, as shown in Figure 4. The sediments in different phases have essentially the same distribution curve: steeper in the La−Eu profile and flatter in the Eu−Lu profile with a right−sloping pattern and a distinct Eu negative anomaly. It has the characteristics of REEs in the continental crust, and the fractionation characteristics are relatively close to those of acidic rock types [71,72]. As shown in Figure 4d, the chondrite−normalized REE patterns of samples in the section have a high morphological similarity with the XiaShu loess in South China [67] and the Yangtze River fluvial sediments (YR) [68]. It differs slightly from northern Chinese Maran loess [69] and Indian wind−formed loess [70].

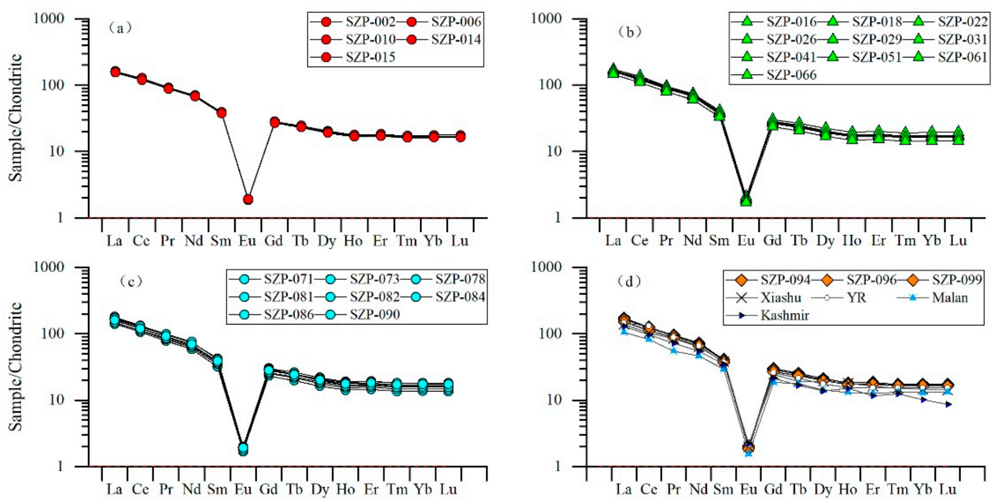

Figure 4. (**a**–**c**): representing the chondrite−normalized REE pattern of sediments from the SZP section in stages I, II, and III, respectively. (**d**): the chondrite−normalized REE pattern in stage IV with the comparison of that in the Xiashu loess (data from [67]), the Yangtze River fluvial sediments (YR), (data from [68]), northern Chinese Maran loess (data from [69]), and Indian wind−formed loess(data from [70]).

4.4. Parameter Characteristics and Paleoenvironment Proxies

In Figure 3 and Table 4, the variations with the depth of REE characteristic parameters are depicted. The LREE content ranges from 183.2 to 230.6 mg·kg^{-1}, with a mean value of 211.31 mg·kg^{-1}, accounting for 89.7% of ΣREE, which is relatively enriched, whereas the HREE content ranges from 20.13 to 24.25 mg·kg^{-1}, with a mean value of 24.25 mg·kg^{-1}, which is somewhat deficient. The LREE/HREE value ranges from 8.2 to 9.4, with a mean value of 7.8, thus indicating enrichment of LREE compared to HREE, consistent with the chondrite−normalized REE patterns Figure 4. The average $(La/Sm)_N$ value is 4.2, reflecting the apparent fractionation of LREE. Similarly, the standard $(Gd/Yb)_N$ value is 1.65, thus signifying a relatively weak fractionation of the HREE. The δEu from the SZP section varies from 0.54 to 0.61, with an average value of 0.58 and medium negative anomalies. The maximum and minimum values of δEu are found in stage III. The LREE/HREE ratio shows two peaks in stage III, reflecting the enrichment of LREE. In most stages, ΣREE follows the same trend as LREE/HREE, $(La/Sm)_N$. Except for stage II−2, the peak of ΣREE (256.2 mg·kg^{-1}) corresponds to the valley of LREE/HREE(8.4) and $(La/Sm)_N$(4.2), implying a rise in the content of HREEs.

Table 4. Parameter characteristics of REEs and element ratios as Paleo−redox proxies, and Paleoclimate proxies in the SZP profile (The unit of Sr is mg·kg^{-1}).

Stage		L/H	δEu	δCe	$(La/Sm)_N$	$(La/Yb)_N$	$(Sm/Nd)_N$	$(Gd/Yb)_N$	Ce/La	V/(V + Ni)	Sr	Rb/Sr
I	Max	8.8	0.59	1.01	4.2	9.6	0.6	1.7	2.07	0.65	49.97	3.67
	Min	8.6	0.57	0.99	4.1	9.1	0.6	1.6	2.01	0.64	47.93	3.42
	Mean	8.7	0.58	0.99	4.2	9.4	0.6	1.6	2.03	0.65	49.10	3.56
II−1	Max	8.9	0.59	1.01	4.3	9.7	0.6	1.7	2.06	0.66	51.95	3.71
	Min	8.8	0.57	0.99	4.2	9.5	0.5	1.6	2.01	0.65	48.04	3.48
	Mean	8.8	0.58	1.00	4.2	9.6	0.5	1.7	2.03	0.65	49.12	3.58
II−2	Max	9.1	0.60	1.01	4.4	10.0	0.6	1.6	2.06	0.68	53.45	3.69
	Min	8.4	0.58	0.96	4.2	8.9	0.5	1.6	1.95	0.65	48.52	3.39
	Mean	8.7	0.59	0.99	4.3	9.4	0.5	1.6	2.01	0.66	50.34	3.54
III	Max	9.4	0.61	0.97	4.4	11.0	0.6	1.8	2.00	0.67	55.44	3.71
	Min	8.2	0.54	0.95	3.9	8.8	0.5	1.5	1.94	0.62	45.57	2.80
	Mean	8.8	0.57	0.97	4.2	9.8	0.6	1.7	1.97	0.65	49.42	3.50
IV	Max	8.6	0.58	0.95	4.2	10.0	0.6	1.7	1.93	0.65	52.72	3.67
	Min	8.3	0.57	0.94	4.1	9.1	0.6	1.6	1.91	0.60	48.75	3.46
	Mean	8.5	0.58	0.94	4.2	9.6	0.6	1.7	1.92	0.64	50.40	3.60
SZP	Max	9.4	0.61	1.12	4.4	11	0.6	1.8	2.07	0.68	55.44	3.71
	Min	8.2	0.54	0.92	3.9	8.8	0.5	1.5	1.91	0.60	45.57	2.80
	Mean	8.7	0.58	1.03	4.2	9.6	0.6	1.6	1.99	0.65	49.64	3.54
Xiashu		8.3	0.64	0.92	3.7	9.6	0.6	1.7				
YR		9.6	0.68	1.12	3.9	9.5	0.6	1.7				
Malan		8.1	0.64	1.03	3.6	8.1	0.6	1.4				
Kashmir		9.8	0.78	0.95	3.8	12.8	0.6	2.1				
Limestone		7.4	0.76	0.83	4.2	8.7	0.6	1.5				
Granite		22.9	0.58	0.94	5.8	45.4	0.5	3.8				
SR		6.8	0.65	0.96	3.3	6.6	0.6	1.4				

The δCe value of the SZP section ranges from 0.94 to 1.01, with an average value of 0.98. The average δCe is the lowest in IV (0.94), followed by those in stage III (0.97), II−2 (0.99), I (0.99), and II−1 (1.00). There is slight variation at each stage, with either weak or no Ce anomalies. Specifically, the average V/(V + Ni) ratio is the lowest in IV (0.64), followed by those in stage III (0.65), II−1 (0.65), I (0.65), and II−2 (0.66). The average value of Ce/La is the lowest in stage IV (1.92), followed by those in stage III (1.97), II−2 (2.01), I (2.03), and II−1 (2.03) successively. It can be inferred that the distribution trend of δCe and Ce/La is the same. The average Rb/Sr ratio is the highest in stage IV (3.6), followed by those in stages II−1 (3.58), I (3.56), II−2 (3.54), and III (3.5), alternately. On the contrary, the average Sr reaches its peak in stage IV (50.4), followed by those in stage II−2 (50.34), III (49.42), I (49.1), and II−1 (48.12), respectively.

4.5. Grain Size Distribution

The particle size results illustrated that the mean grain size (Mz) was 6.5–7.5 μm, with an average value of 7.1μm. The mean value of stage III is the smallest, while stage II is the largest. The sediments in the study area are dominated primarily by silty clay (average volume fraction of 65%).

5. Discussion

5.1. The Paleo−Hydrological Reconstruction of the Xiangjiang River

In oxidation conditions, Ce^{3+} can be easily oxidized to 4−valent CeO_2 and separated from other trivalent REEs [73]. The δCe can sensitively reflect the redox condition of the deposition environment, with a value range of >1, indicating an oxygen−rich environment and a value range of <1 showing a reduced environment [73]. Where Ce/La > 2 represents a reduced environment, and <1.5 means an oxygen−rich environment [73]. The V is an element sensitive to redox conditions, deficient in the sediment of oxidizing environments, and enriched in reducing environments [59,60]. Previous studies have demonstrated that V/(V + Ni) ratio is positively correlated with reducibility [15,74]. V/(V + Ni) >0.84 represents an anaerobic environment with stratified water bodies, with values 0.6–0.84 indicating weak water stratification in the anoxic environment and values <0.6 indicating an oxygen−rich sediment environment [15,60]. Generally, Sr and Rb/Sr ratios are the critical approaches to determining paleoclimate [54]. The Sr is a typical dry element, with low concentrations indicating a humid climate and high concentrations representing a dry environment [61]. During weathering, the geochemistry of Rb is relatively stable, while Sr is more likely to be leached or oxidized. In warm and humid climates, weathering leads to excessive leaching of Sr elements, increasing the Rb/Sr ratio. In arid climates, less precipitation and weaker weathering can preserve Sr intact, giving rise to lower Rb/Sr ratios [62].

The SZP section recorded the sedimentary sequence of the Shizhu area over the past 1300 years (Figure 2). It was asserted that a commercial wharf connected to the Xiangjiang River existed in the Shizhu area in the mid−9th century AD, with direct access to the Yangtze River [74]. The hydrological environment of Xiangjiang River should be comprehensively analyzed from the perspective of climate and water level change in the Central Yangtze River. The paleo−hydrological evolution was categorized into four main stages based on REE characteristics, element ratio, and lithofacies.

Stage IV (>310cm): The Loess layer thickness of >1m was developed in the SZP sections. The lowest value of the redox proxies, δCe (0.94), V/(V +Ni) (0.64), and Ce/La (1.92), all appeared in this stage (Figure 5b–d). Low Ce anomaly and V/V+Ni mean low water level [15,60]. Correspondingly, The highest values of the climate proxies, Rb/Sr ratio (3.6) and Sr (50.4), also emerged in stage IV and meant that the climate was cold and dry [54,61]. These properties are interpreted to indicate that under the dry and cold climate at that time, the reduction of precipitation reduced the water level of the Xiangjiang River. During the Late Pleistocene, the global climate was dominated by dryness and coldness, accompanied by a significant reduction in sea level and exposure of the continental shelf to form land [75,76]. The decrease in the water level of the Xiangjiang River led to an increase in the erosion capacity of the river channel undercutting and a deepening of the river valley [77]. A large amount of dust was generated, with solid winter winds eroding the river valley and floodplain [78]. Loess began to accumulate on the surrounding terraces. The Dongting Lake area reflected a geomorphic landscape with alluvial plains, river valleys, and River network cutting plains [77] (Figure 6a). After the end of the last glacial, the sea level rebounded rapidly and reached the level of the current sea level at around 6000 a.BP, and the water level of the Yangtze River rose rapidly [79]. The extent of the Dongting Lake lake area gradually expanded, and the lake area within the lake basin reached 5000–6000 km^2 [80] (Figure 6b).

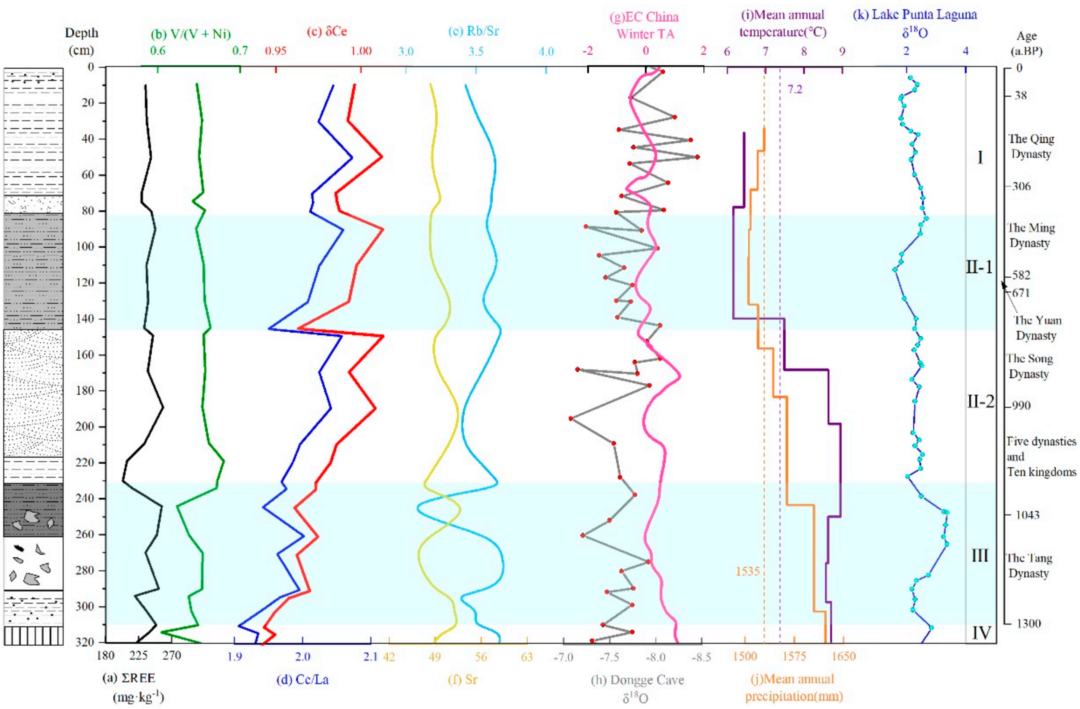

Figure 5. (**a**): Vertical distribution trend of ∑REEs in the SZP profile. (**b**–**d**): Variations of paleo−redox environment proxies(δCe, Ce/La, V/(V + Ni)). (**e**,**f**): Characteristics of the paleoclimate proxies (Rb/Sr, Sr, the unit of Sr is mg·kg^{-1}) in the SZP section. (**g**): The winter half−year temperature anomaly (TA) for central−eastern (EC) China, adapted form [81]. (**h**): the δ^{18}O values from stalagmites Dongge cave, adapted from [82]. (**i**–**j**): Temperature and precipitation curves based on sporulation data from Lake Dajiu in Central Yangtze River. Vertical lines represent modern annual temperature (7.2 °C) and precipitation(1535 mm), adapted form [83]. (**k**): Sediment cores from Lake Punta Laguna, northern Yucatan Peninsula, Mexico, adapted form [84]. The blue shaded area represents the high water level period in the Xiangjiang River Basin. Except for 1300 a.BP, the nodes are the extinction time of the dynasty, adapted form [81].

Stage III (310–230cm, 1288–1094 a.BP): The lithology was dominated by Yellowish gray clay to Gray mud. The redox indexes (δCe = 0.97, Ce/La = 1.97, V/(V + Ni) = 0.65) (Table 4) displayed the anoxic environment and high water [15,60]. Rb/Sr and Sr trends showed a humid environment (Figure 5e–f). The transition from raw soil to Gray mud indicated that the rising water level of the Xiang River eroded the Shizhu area and formed lakes. Stage III is a cultural layer of the Tang Dynasty. Many pottery shards reflected the prosperity of the porcelain−making industry of Changsha kiln in the Tang Dynasty. The Chronological results of the cultural layer were roughly consistent with the existing ceramic archaeological findings of the Changsha kiln (1184–990 a.BP) [74]. During 1409–1210 a.BP (the Early Tang Dynasty), the warming in China was more pronounced than in the Northern Hemisphere [85,86]. The δ^{18}O values from stalagmites Dongge cave (Figure 5h) [82] and the mean annual temperature (Figure 5j) [83] show that China maintained a temperate climatic environment under the control of the East Asian summer winds at about 1100 a.BP. Based on lithology, redox proxies, and climate proxies, we suggested that due to the influence of the East Asian monsoon, the climate of the Tang Dynasty was warm and humid. High precipitation made the water level of the Xiangjiang River rose, and lakes appeared in the Shizhu area. The porcelain industry of Changsha kiln flourished around the lake (Figure 6c). The SZP section was located on the river terrace, which was 8–13 m higher than the river's surface. The annual water level of the Changsha area in the Xiangjiang River fluctuates between 29–31 m [22,87]. It can be concluded that only when the water level of the Xiangjiang River reaches at least 37 m can a lake be formed in the profile (Figure 6c).

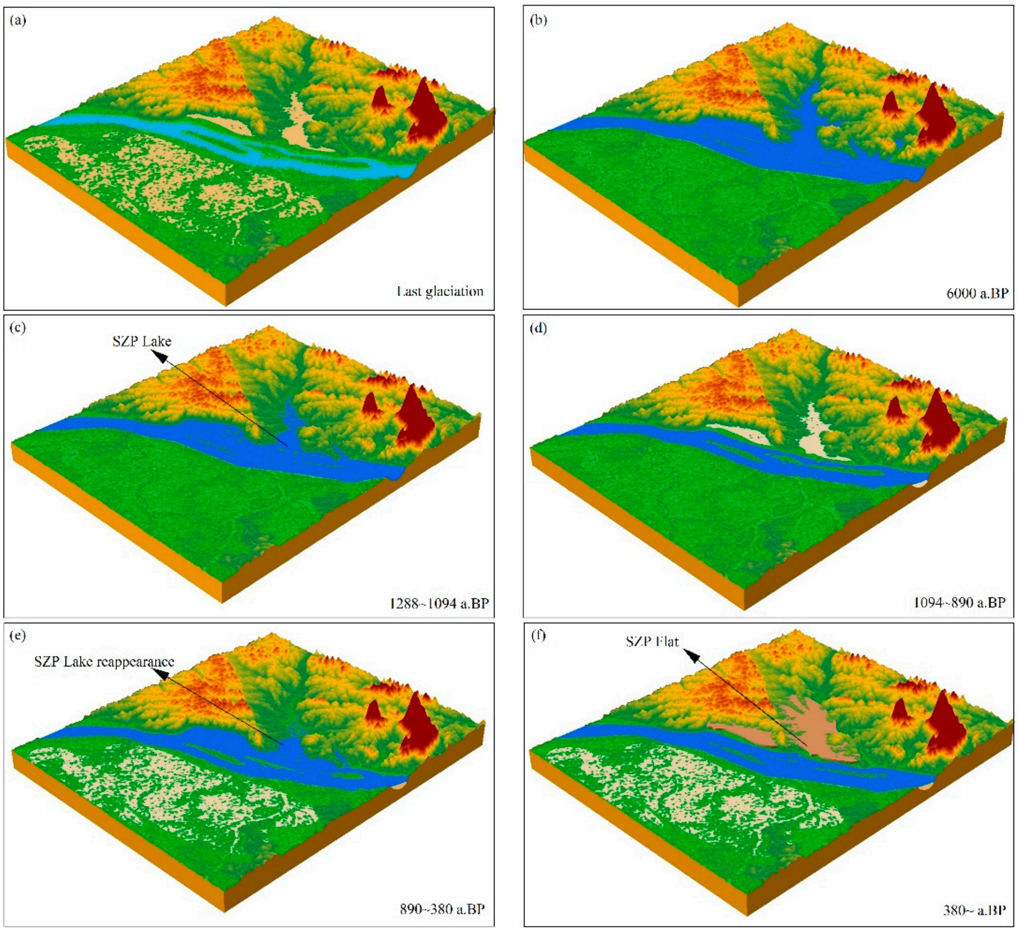

Figure 6. Evolution of the palaeohydrological environment in the Xiangjiang River basin. (**a**): During the last glacial period, the watershed was a river−cut plain landscape. (**b**): At 6000 a.BP, the Yangtze River reached its highest water level. (**c**): 1288–1094 a.BP, the climate was warm and humid. The Xiangjiang River was at a high−water period, and lakes appeared in the Changsha Kiln area. (**d**): 1094–890 a.BP, the climate turns dry and cold. The water level of the Xiangjiang River dropped, the lake disappeared, and the floodplain appeared. (**e**): 890–380 a.BP, the Xiangjiang River bed was raised, the water level rose, and a shallow lake appeared in the kiln area. (**f**): 380–a.BP, Dikes were built in the Changsha kiln area and flats were formed around the SZP profile.

The Rb/Sr maintained a stable trend until a sharp decline at 225–223 cm (1082 a.BP–1077 a.BP) (Figure 5e–f). The Sr showed a minimum value (45.57), whereas Rb/Sr showed a maximum value (3.71), indicating that the climate became dry. Sporopollen records in the central Yangtze River showed that precipitation gradually decreased in the late Tang Dynasty (1043a. BP) (Figure 5j). Yancheva (2007) [88] suggested that the prolonged drought caused by the strengthening of winter winds and the weakening of summer winds brought about the downfall of the Tang Dynasty, which echoed the stalagmite $\delta^{18}O$ record [81] (Figure 5h). The continuous drought in Mexico during 1150–950 a.BP brought about the decline of the Mayan civilization (Figure 5k) [84]. The rainfall decreased after the climate became dry, resulting in the decline of the water level of the Xiangjiang River. The lakes in the Shizhu area gradually dried up, and the river sand continued to accumulate to form a floodplain. There were no cultural relics of human activities in Stage II−2, indicating that the kilns around the lake were abandoned during this period.

Stage II−2 (230–145 cm,1094–890 a.BP): The lithology of the stratum was clay and Silty clay, and its sedimentary stage was a river floodplain (Figure 6d). The color change of stage II−2 may suggest that the water level of the Xiangjiang River was lower than that of Stage III. However, in late−stage II−2, the water level gradually increased. The δCe value was gradually increased (0.96–1.01), and the depositional environment gradually changed from an oxygen−rich to a reducing environment [89]. From the Five Dynasties to the early Song Dynasty, China experienced an extended cold period (Figure 5i–g). The $\delta^{18}O$ isotopic records of Dongge Cave stalagmites [82] implied that the middle of the Northern Song Dynasty (920–520 a.BP) was a cold climatic period and a critical turning point in climate change (Figure 5h). When the climate was dry in the Five Dynasties (1043–990 a.BP), the lakes in Changsha kiln disappeared. The surface height of the flood plain around Xiangjiang River was 0–5 m higher than that of Xiangjiang River [22]. When the lakes in the Shizhu area disappeared, the water level of the Xiangjiang River was no more than the minimum value of the annual average water level (29 m).

Stage II−1 (145–80 cm, 890–380 a.BP) was a black silt layer with bog facies deposits. According to the value of δCe (1.00) and Ce/La (2.03), it could be assumed to be in a reducing environment. Shizhu Lake reappeared in the late Song Dynasty (890 a.BP). The construction of dikes in the central Yangtze River gradually ameliorated from the Eastern Jin Dynasty (1633–1530 a.BP) to the middle of the Song Dynasty (930–870 a.BP) [90]. After strengthening the dikes, many floodwaters carrying sediment entered the Dongting Lake area. The gradual siltation of the main tributaries of the Yangtze River and the low−lying areas on both sides of the river, together with the construction of dikes, gave birth to a continuous rise in the water level of the Yangtze River, which prevented the drainage of water and sand in the Dongting Lake area [91]. The riverbed of Xiangjiang River rises constantly, and Shizhu Lake gradually silts up, forming a shallow lake again (Figure 6e). The reformation of Shizhu Lake indicated that the water level reached more than 37 m above again.

Stage I: Above 80 cm lies the anthropogenic bedding and topsoil layer: the stratum contains gravel, gray pottery flakes, and red−burned soil. After the disappearance of the Changsha kiln in the Tang Dynasty, some people made porcelain in the kiln area, but the technology and style were different from before. In 1964 a.AD, the excavation of the new river in Shizhu and the dike construction activities in the area from Tongguan Town to Shizhu demolished some of the kiln sites [74]. The SZP gradually formed the flat (Figure 6f). The pottery flakes and red−burned soil in the sediment above 80 cm are mainly related to human activities. At this stage, the water level of the Xiangjiang River was basically the same as that of the current water level.

5.2. Provenance Discrimination

5.2.1. Control Factors of REEs Composition

The REEs are inactive during the weathering, transport, and deposition and mainly host and maintain the original properties of the source [92]. In addition to the bedrock composition of the source rock, factors such as grain size, minerals, and diagenesis, can also affect the REE composition of the sediments [93,94]. It is necessary to evaluate the constraints affecting the composition of REEs when using REEs for sediment source tracing.

Previous research results concluded that REEs are mainly enriched in clay grain−level sediments <2 μm [95]. It can also be seen in clay minerals in the form of rare earth−rich minerals, such as oxides of Ti and apatite [96]. To further investigate the Particle size effect of sediments, a correlation analysis of sediment particle size with the characteristic parameters of rare earth elements was carried out (Figure 7). The correlation coefficients of ∑REEs with the Mz (−0.24), clay (−0.23), silt (0.12), and sand (0.25) indicate that there is no significant correlation between them. Therefore, the REE content of SZP sediment is not controlled by particle size. The results are consistent with the sediment from the Major Tributaries and the Main Stream of the Yangtze River [97].

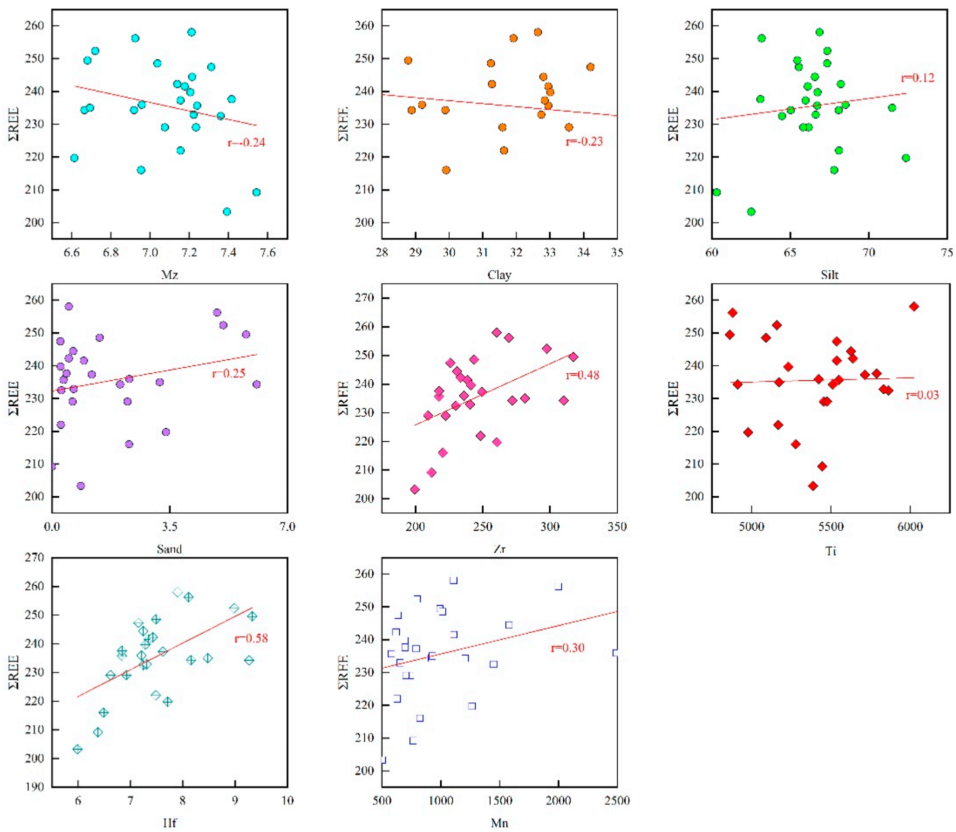

Figure 7. Correlation and linear regression curves of ΣREE with Mz, Mn, Ti, Zr, and Hf.

In addition, mineral composition is also one of the critical factors influencing the REE characteristics of deposits [91]. Rare earth−rich heavy mineral fractions lead to higher REE content in sandy sediments [98]. LREEs are more abundant than HREEs in heavy minerals, including titanite, hornblende, limonite, apatite, and monazite. Simultaneously, HREEs tend to be enriched in zircon, tourmaline, garnet, and other minerals [99,100]. The correlation of ∑REE with stable heavy elements Zr (0.48), Hf (0.58), and Mn (0.3) is weak, and the correlation with heavy mineral elements Ti (0.03) is not significant. It indicates that the composition of REEs in the sediments is weakly correlated with heavy minerals. In summary, the source rock plays a significant role in controlling the distribution of REEs from the SZP section.

5.2.2. Provenance Inferred from the REEs Characteristics

The geological structure of the Xiangjiang River basin is that carbonate rocks account for about 60% of the exposed area, and granites constitute about 2% (Figure 8a). In general terms, clastic sedimentary rocks, carbonate rocks, and granites may be sediment sources in the Xiangjiang river basin [54]. The projected values of REE contents on the La/Yb−∑REE diagram (Figure 8b) mostly fall at the intersection of sedimentary rocks, granites, and basalts. It meant that the parent rocks of the SZP profile might be mainly sedimentary rocks and granites.

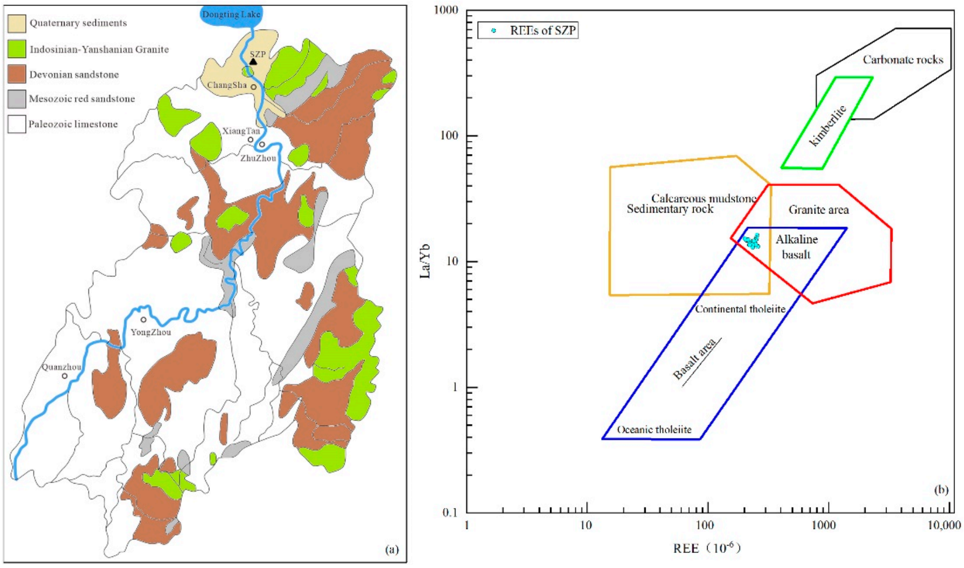

Figure 8. (**a**): Geological background tectonic map of the lower reaches of Xiangjiang River, adapted from [54]. (**b**): Distribution of samples on La/Yb−∑REE diagram [100].

Stage IV: The chondrite−normalized REE patterns in the SZP section are highly consistent with the XiaShu loess and the Yangtze River floodplain deposits (YR). In contrast, there were slightly different from the Maran loess and the Indian wind−formed loess, reflecting that they are wind−formed accumulations of similar origin to the Xiashu loess (Figure 4d). The similarity of REEs content corroborates this (Table 3). The mean value of stage IV (236.8 mg·kg^{-1}) is relatively close to that of the Xiashu loess (207.7 mg·kg^{-1}) and the Yangtze River diffuse sediment (233.6 mg·kg^{-1}) and much higher than that of the Malan loess (159.2 mg·kg^{-1}) and Kashmir loess (186.5 mg·kg^{-1}). During the Late Pleistocene, the Xiashu loess of the middle and lower reaches of the Yangtze River in China was initially thought to be a river and lake deposit. However, recent studies have confirmed a wind deposit [101]. A current consensus is that the Xiashu loess is not remote provenance but has an indigenous origin [63], transported by the wind system. It can be inferred that stage IV is a typical Xiashu loess layer. The material source is the weathering accumulation of riverine sediments from the middle and lower reaches of the Yangtze River.

Stage III (1288–1094 a.BP): Abundant ceramic pieces and braised clay in the cultural layer indicated the frequent porcelain−making activities in Changsha kilns during this period. According to ceramic archaeology, the Changsha kiln reached its peak in the porcelain trade in the middle and late Tang Dynasty (1195–1043 a.BP) [25]. The ΣREE of stage III had the largest change in all stages, and LREE/HREE, $(La/Sm)_N$ had the same trend (Figure 3). The enrichment of LREE implied an increase in minerals such as apatite [99]. The Changsha kilns featured ceramics with copper−red glazed porcelain. The glaze of porcelain adopts apatite and calcite as flux. Cu, Fe, Mn, and other minerals are used as colorants for the glaze [74]. During porcelain production, a large amount of waste residue was dumped into the lakes in the kiln area, increasing REEs in sediments. The average value of ΣREEs in the Changsha kiln porcelain samples was 228.5 mg·kg^{-1} [30]. Among all stages, the mean value of ΣREE in stage III (233.3 mg·kg^{-1}) was closest to the porcelain (228.5 mg·kg^{-1}). Therefore, the slag produced by porcelain−making activities was the main source of stage III. During the Five Dynasties (1043–990 a.BP), the lake dried up, and the Changsha kiln was abandoned. The suspension of porcelain−making activities was the main reason for the sharp decline of the ΣREE in the late stage of stage III (225–223 cm, 1082–1077 a.BP).

Stage II (1094–380 a.BP): The provenance of this layer was divided into two parts according to stratigraphy and vertical distribution trend of elements. The stage II−2 (1094–890 a.BP) was mainly river floodplain deposits, mainly from the sediment imported in large quantities from the Xiangjiang River. The mean elemental value of this layer is growing, but the ratio of LREEs to HREEs is shrinking, which indicates that the percentage of HREEs has increased (Figure 5). Zircon has the characteristic of being rich in HREE [102]. As mineral weathering enhances, Zr and Hf migrate and are retained only as zircon [103]. Zircon was dispersed in igneous rocks and widely existed in granitic ores [104]. The relatively significant correlation of ΣREE with Hf and Zr shows that the primary source of this layer was the granite distributed in the middle−lower reaches.

The depositional environment of stage II−1(890–380a.BP) was more enclosed. The ΣREE had the least changes reflecting the gradual stabilization of the water level of Shizhu Lake and the fall in the contribution of sediment from the Xiangjiang River. The mean value of ΣREE in stage II−1 (240.8 mg·kg^{-1}) was more than that in stage II−2 (235.7 mg·kg−1), and the proportion of LREE increased. The sedimentary rocks in the Hunan area are characterized by high REE abundance and large LREE/HREE (8.4) and (La/Sm) N ratio [59]. Accordingly, it can be seen that the components containing sedimentary rocks, such as sandstone shale, began to be imported into Shizhu Lake after the water level of the Xiangjiang River rose. The source was mainly from the weathering and denudation of sandstone, which was widely distributed in the middle−lower reaches.

Stage I (380–a.BP): The average value of ΣREE (234 mg·kg^{-1}) was similar to that of the SZP section (235.6 mg·kg^{-1}), and many gravels and wormholes indicated they were frequently eroded by flowing water. The distribution of all REEs in this layer was almost unchanged, and the fractionation pattern and characteristic parameters were homogeneous (Figures 4a and 5), indicating a single source. The mean value of δEu (0.58) was closest to granite (0.58). After forming the SZP flat, the influence of Xiangjiang River sediment on stage I could be neglected. Based on the inheritance of δEu to the original rocks [105], and Granite and Quaternary alluvium were the nearest lithological distribution to the study area, it could be judged that the material source was mainly granite (Figure 8a). The SZP flat was used as a dike now, and the alluvium was unsuitable as a raw material. Its components were artificial matting made from soils taken from the surrounding area during the construction of embankments and the weathered erosion accumulation of the surrounding slope rocks.

5.3. Impacts of Hydrological Change on the Changsha Kiln Development

The analysis of climate and hydrological environment evolution and provenance provided an essential basis for the derivation of human activities in The Changsha kiln in the Tang Dynasty. The relationship between the development of the Changsha kiln and the environment can be further analyzed based on historical documents.

In Stage III (310–230 cm, 1288–1094 a.BP), China maintained a warm and humid climate under the control of the East Asian monsoon, and the Xiangjiang River was in a period of high water level due to high rainfall. In 1195 a.BP, a national war broke out in China, and many northern immigrants fled to the south [28,86]. Changsha was one of the southern Chinese political, cultural, and economic centers and attracted many immigrants [86]. The northern immigrants enter Dongting Lake Basin with the help of the Yangtze River system and then enter Shizhu Area through the Xiangjiang River Basin [21]. Northern kiln workers among the immigrants brought new technology and labor force to Changsha kiln. The Changsha kiln broke away from the Yuezhou kiln system [25] and produced internationally oriented goods [24]. In 1988, more than 56,500 pieces of Tang Dynasty Changsha kiln porcelain fragments were found on black rocks in the South China Sea, marking the heyday of Changsha kiln foreign trade [24]. The high water level of the Xiangjiang River was a prerequisite for immigrants entering the Shizhu, while merchants had established commercial docks on the lake (Figure 6c) [25,28].

In Stage II−2 (1094–890 a.BP), the dry climate and reduced rainfall caused the water level of the Xiangjiang River to drop (Figure 6d). The lakes in the kiln area disappeared to form a floodplain, and the Changsha kiln was abandoned. From the Five Dynasties to the Song Dynasty, the center of gravity of Chinese ceramic exports began to shift to the coast [27], and the Changsha kiln located inland lost its overseas markets. However, the Changsha kiln also had a domestic market in China [74], and the loss of overseas markets does not convincingly explain the abandonment of the kiln site. The recession of the Xiangjiang River water level was one of the factors that led to the abandonment of the Changsha kilns. The kiln site in the Shizhu area was not connected to the Xiangjiang River and directly lost its function as a commercial dock, affecting the waterway transportation and market exchange for the Changsha kiln. At the same time, the war began to breed because of the dry climate that led to agricultural damage in the Changsha area [106]. The Changsha kilns were challenging to maintain amid the war.

6. Conclusions

In this investigation, the evolutionary history of the paleo−hydrological environment and provenance at the Changsha kiln since 1300 a.BP was reconstructed based on the analysis of REEs and trace elements ratio in the sedimentary records of the SZP section. The findings clearly indicate that during the last glacial period, the geomorphic landscape of the Shizhu area was dominated by river valleys and river network cutting plains. The provenance of the SZP section was mainly aeolian accumulation. The climate in the early Tang Dynasty was warm and humid under the influence of the East Asian summer monsoon. Higher rainfall caused the water level of the Xiangjiang River to rise, and the northern migrants entered the Shizhu area by boat. Changsha kiln began to flourish after receiving technology and labor from the north. The waste from ceramic production has entered the SZP section. Then the monsoon declined, the water level of the Xiangjiang River dropped under the dry cold climate, and The Shizhu area lost its function as a commercial dock. Changsha kiln was abandoned, and the provenance of the SZP section became the denudation of granite in the middle and lower reaches of the Xiangjiang River. Subsequently, during the Northern Song Dynasty (890–380 a.BP), the climate warmed up, and the water level of the Xiangjiang River gradually rose. However, the sediment brought by the dam's construction raises the riverbed and makes the lake shallower. Sedimentary rocks become the primary source of the provenance of the section. In 1988, a dike was built in the Shizhu area to form a flat landscape. The results of this study illustrate the dynamic interactions between the hydrological environment, sources, and human activities, providing valuable insights to help better understand the paleoenvironmental influences and constraints on the development of Changsha kilns.

Author Contributions: Conceptualization, methodology, writing, software, visualization, A.G.; Conceptualization, writing, supervision, L.M.; investigation, resources, S.S. and X.Z.; project administration, funding acquisition, D.M. All authors have read and agreed to the published version of the manuscript.

Funding: This research was funded by the National Social Science Major Foundation of China, grant number: 19ZDA231; The National Natural Science Foundation of China, grant number: 41771218; The National Key Research and Development Program of China, grant number: 2020YFC1521605.

Institutional Review Board Statement: Not applicable.

Informed Consent Statement: Not applicable.

Data Availability Statement: Not applicable.

Acknowledgments: We would like to thank the handling editor and the two reviewers for their constructive comments, which considerably improved this paper.

Conflicts of Interest: The authors declare no conflict of interest.

References

1. Caseldine, C.J.; Turney, C. The bigger picture: Towards integrating palaeo−climate and environmental data with a history of societal change. *J. Quat. Sci.* **2010**, *25*, 88–93. [CrossRef]
2. Zhang, J.; Chen, F.; Holmes, J.A.; Li, H.; Guo, X.; Wang, J.; Li, S.; Lu, Y.; Zhao, Y.; Qiang, M. Holocene monsoon climate documented by oxygen and carbon isotopes from lake sediments and peat bogs in China: A review and synthesis. *Quat. Sci. Rev.* **2011**, *30*, 1973–1987. [CrossRef]
3. Heyvaert, V.; Baeteman, C. A Middle to Late Holocene avulsion history of the Euphrates river: A case study from Tell ed−Dēr, Iraq, Lower Mesopotamia. *Quat. Sci. Rev.* **2008**, *27*, 2401–2410. [CrossRef]
4. Benito, G.; Macklin, M.G.; Cohen, K.M.; Herget, J. Past hydrological extreme events in a changing climate. *Catena* **2015**, *130*, 1–2. [CrossRef]
5. Kittel, P.; Sikora, J.; Antczak, O.; Brooks, S.J.; Elias, S.; Krapiec, M.; Luoto, T.P.; Borówka, R.K.; Okupny, D.; Pawłowski, D.; et al. The palaeoecological development of the late medieval moat—Multiproxy research at rozprza, central poland. *Quat. Int.* **2018**, *482*, 131–156. [CrossRef]
6. Altaweel, M. Water management across time: Dealing with too much or too little water in ancient Mesopotamia. In *Water Societies and Technologies from the Past and Present*; UCL Press: London, UK, 2018; pp. 180–199.
7. Geirsdottir, A.; Miller, G.; Larsen, D.J.; Olafsdottir, S. Abrupt Holocene climate transitions in the northern North Atlantic region recorded by synchronized lacustrine records in Iceland. *Quat. Sci. Rev.* **2013**, *70*, 48–62. [CrossRef]
8. Staubwasser, M.; Weiss, H. Holocene climate and cultural evolution in late prehistoric−early historic West Asia. *Quat. Res.* **2006**, *66*, 373. [CrossRef]
9. Riehl, S. Variability in ancient Near Eastern environmental and agricultural development. *J. Arid Environ.* **2012**, *86*, 113–121. [CrossRef]
10. Sionneau, T.; Bout−Roumazeilles, V.; Biscaye, P.E.; Vliet−Lanoe, B.V.; Bory, A. Clay mineral distributions in and around the mississippi river watershed and northern gulf of mexico: Sources and transport patterns. *Quat. Sci. Rev.* **2008**, *27*, 1740–1751. [CrossRef]
11. Kerr, P.J.; Tassier, S.A.; Kilgore, S.M.; Bettis, E.A.; Cramer, B.D. Timing, provenance, and implications of two MIS 3 advances of the Laurentide Ice Sheet into the Upper Mississippi River Basin, USA. *Quat. Sci. Rev.* **2021**, *261*, 106–926. [CrossRef]
12. Liu, F.; Feng, Z. A dramatic climatic transition at ~4000 cal. yr BP and its cultural responses in Chinese cultural domains. *Holocene* **2012**, *22*, 1181–1197. [CrossRef]
13. Wu, L.; Li, F.; Zhu, C.; Li, B. Holocene environmental change and archaeology, Yangtze River Valley, China: Review and prospects. *Geosci. Front.* **2012**, *3*, 875–892. [CrossRef]
14. Crowley, T.J. Causes of climate change over the past 1000 years. *Science* **2000**, *289*, 270–277. [CrossRef] [PubMed]
15. Jones, B.; Manning, D.A.C. Comparison of geochemical indices used for the interpretation of palaeo−redox conditions in ancient mudstones. *Chem. Geol.* **1994**, *111*, 111–129. [CrossRef]
16. Alley, R.B.; Mayewski, P.A.; Sowers, T.; Stuiver, M.; Taylor, K.C.; Clark, P.U. Holocene climatic instability a prominent, widespread event 8200 yr ago. *Geology* **1997**, *25*, 483. [CrossRef]
17. Wanner, H.; Beer, J.; Butikofer, J.; Crowley, T.J.; Cubasch, U.; Fluckiger, J. Mid−to−late Holocene climate change: An overview. *Quat. Sci. Rev.* **2008**, *27*, 1791–1828. [CrossRef]
18. Innes, J.B.; Zong, Y.; Wang, Z.; Chen, Z. Climatic and palaeoecological changes during the mid− to late holocene transition in eastern china: High−resolution pollen and non−pollen palynomorph analysis at pingwang, yangtze coastal lowlands. *Quat. Sci. Rev.* **2014**, *99*, 164–175. [CrossRef]
19. Jones, M.; Liu, X. Origins of agriculture in East Asia. *Science* **2009**, *324*, 730–731. [CrossRef]
20. Deng, C.; Zhu, D.; Liu, Y.; Li, Z. Spatial matching and flow in supply and demand of water provision services: A case study in Xiangjiang River Basin. *J. Mt. Sci.* **2022**, *19*, 228–240. [CrossRef]
21. Guo, Y.; Mao, L.; Mo, D.; Shu, J.; Guo, A. Vegetation dynamics and human activities over the past 1300 years revealed by pollen record at the Tongguan kilns, lower Xiangjiang River, China. *Quat. Int.* **2020**, *577*, 139–146. [CrossRef]
22. Luo, Q. The Study of the Quaternary Environment of the Dongting Lake and the Upper Xiangjiang. Master's Thesis, College of Tourism Central China Nomral Unlversity, Wuhan, China, 2001.
23. Janice, S. Indian Ocean Trade in the Ninth and Tenth Centuries: Demand, Distance, and Profit. *South Asian Stud.* **2014**, *30*, 35–55.
24. Abaei, M.; Jaafarnia, M. Where Was the Destination of Black Stone Shipwreck: Comparative Study on Founded Products in Iran and Products of Black Stone. In Proceedings of the New Silk Road Program of the Conference Hunan University, Changsha, China, 20 May 2015.
25. Li, B. On several problems of Changsha Kiln porcelain. *Palace Mus. J.* **1985**, *1*, 70–73.
26. Shen, B.; Philippe, S.; Tian, W.; Magali, B.; Li, J.; Wen, L.; Zhu, T. Micro−structural study of colored porcelains of Changsha kiln using imaging and spectroscopic techniques. *Ceram. Int.* **2018**, *44*, 18528–18534. [CrossRef]
27. Deng, J. Records of Changsha Kiln. *Ceram. Sci. Art* **2017**, *51*, 85–87.
28. Wu, X. *Mysteries of Changsha Kiln*; Guangdong Economic Publishing House: Guangzhou, China, 2016; pp. 2–13.
29. Tan, Z.; Mao, L.; Han, Y.; Mo, D.; Gu, H. Black carbon and charcoal records of fire and human land use over the past Cheek l 1300 years at the Tongguan Kiln archaeological site, China. *Palaeogeogr. Palaeoclimatol. Palaeoecol. Int. J. Geo−Sci.* **2018**, *504*, 162–169. [CrossRef]

30. Mao, L.; Du, J.; Mo, D.; Yang, J.; Gu, H. Rare earth elements geochemistry of ceramics excavated from Tongguanyao site, China. *Adv. Eng. Res.* **2015**, 180–183. [CrossRef]
31. Leybourne, M.I.; Johannesson, K.H. Rare earth elements (REE) and yttrium instream waters, stream sediments, and Fe−Mn oxyhydroxides: Fractionation, speciation, and controls over REE plus Y patterns in the surface environment. *Geochim. Cosmochim Acta* **2008**, *72*, 5962–5983. [CrossRef]
32. Menendez, A.; James, R.H.; Roberts, S.; Peel, K.; Connelly, D. Controls on the distribution of rare earth elements in deep−sea sediments in the north atlantic ocean. *Ore Geol. Rev.* **2017**, *87*, 100–113. [CrossRef]
33. Valentina, C.; Frank, J.M. Distribution of yttrium and rare earths in Florida Bay sediments. *Mar. Chem.* **2007**, *104*, 171–185.
34. Li, C.S.; Shi, X.F.; Kao, S.J.; Liu, Y.G.; Lyu, H.H.; Zou, J.J.; Liu, S.F.; Qiao, S.Q. Rare earth elements in fine−grained sediments of major rivers from the high−standing is land of Taiwan. *J. Asian Earth Sci.* **2013**, *69*, 39–47. [CrossRef]
35. Khan, A.M.; AbuBakar, N.K.; AbuBakar, A.F.; Ashraf, M.A. Chemical speciation and bioavailability of rare earth elements (REEs) in the ecosystem: A review. *Environ. Sci. Pollut. R.* **2017**, *24*, 22764–22789. [CrossRef] [PubMed]
36. Gwenzi, W.; Mangori, L.; Danha, C.; Chaukura, N.; Dunjana, N.; Sanganyado, E. Sources, behaviour, and environmental and human health risks of high−technology rare earth elements as emerging contaminants. *Sci. Total Environ.* **2018**, *636*, 299–313. [CrossRef]
37. Prego, R.; Caetano, M.; Vale, C.; Marmolejo−Rodríguez, J. Rare earth elements in sediments of the Vigo Ria, NW Iberian Peninsula. *Continent. Shelf Res.* **2009**, *29*, 896–902. [CrossRef]
38. Tepe, N.; Bau, M. Behavior of rare earth elements and yttrium during simulation of arctic estuarine mixing between glacial−fed river waters and seawater and the impact of inorganic (nano−) particles. *Chem. Geol.* **2016**, *438*, 134–145. [CrossRef]
39. Nie, Y.; Liu, X.; Emslie, S.D. Distribution and sources of rare earth elements in ornithogenic sediments from the Ross Sea region, Antarctica. *Micro−Chem. J.* **2014**, *114*, 247–260. [CrossRef]
40. Ahn, J.S.; Youm, S.J.; Cho, Y.C.; Shin, S.C.; Cho, W.H. Geochemical survey of rare earth elements (REEs) in the concealed ore body of Hongcheon, Korea. *Environ. Earth Sci.* **2014**, *72*, 2153–2161. [CrossRef]
41. Sdnt, A.; Jna, B.; Vlo, B. Mineralogy and geochemistry of alluvial sediments from the Kadey plain, eastern Cameroon: Implications for provenance, weathering, and tectonic setting. *ScienceDirect. J. Afr. Earth Sci.* **2016**, *163*, 323–348.
42. Liu, X.; Sun, L.; Li, D.; Wang, Y. Rare earth elements in the ornithogenic sediments from the Maritime Antarctic: A potential new palaeo−ecology proxy. *Geochem. J.* **2013**, *45*, 15–26. [CrossRef]
43. Dou, Y.G.; Yang, S.Y.; Liu, Z.X.; Peter, D.C.; Shi, X.F.; Yu, H.; Serge, B. Provenance discrimination of siliciclastic sediments in the middle Okinawa Trough since 30 ka: Constraints from rare earth element compositions. *Mar. Geol.* **2010**, *275*, 212–222. [CrossRef]
44. Reba, B.; Njgpb, C.; Rai, D. Revisiting the provenance of the Stonehenge bluestones: Refining the provenance of the Group 2 non−spotted dolerites using rare earth element geochemistry. *J. Archaeol. Sci. Rep.* **2021**, *38*, 103083.
45. Censi, P.; Sprovieri, M.; Saiano, F.; Geronimo, S.I.D.; Larocca, D.; Placenti, F. The behaviour of REEs in Thailand's Mae Klong estuary: Suggestions from the Y/Ho ratios and lanthanide tetrad effects. *Estuar. Coast Shelf Sci.* **2007**, *71*, 569–579. [CrossRef]
46. Algeo, T.J.; Liu, J.S. A re−assessment of elemental proxies for paleoredox analysis. *Chem. Geol.* **2020**, *540*, 119549. [CrossRef]
47. Yeh, C.; Wu, J.; Lee, G.; Wen, H.; Lin, P.; Kuo, C. Vanadium Derivative Exposure Promotes Functional Alterations of VSMCs and Consequent Atherosclerosis via ROS/p38/NF−κB−Mediated IL−6 Production. *Int. J. Mol. Sci.* **2019**, *20*, 6115. [CrossRef] [PubMed]
48. Jiu, K.; Ding, W.; Huang, W.; Zhang, J.; Zeng, W. Formation Environment and Controlling Factors of Organic−rich Shale of Lower Cambrian in Upper Yangtze Region. *Geoscience* **2012**, *26*, 547–554.
49. Tribovillard, N.; Algeo, T.J.; Lyons, T.; Riboulleau, A. Trace metals as paleo−redox and paleo−productivity proxies: An update. *Chem. Geol.* **2006**, *232*, 12–32. [CrossRef]
50. Algeo, T.J.; Morford, J.; Cruse, S. New Applications of Trace Metals as Proxies in Marine Paleoenvironments. *Chem. Geol.* **2012**, *324–325*, 1–5. [CrossRef]
51. Tao, X.; Chen, H.; Xu, C.; Hou, Y.; Jie, M. Analysis and prediction of reference evapotranspiration with climate change in Xiangjiang River Basin, China. *Water Sci. Eng.* **2015**, *8*, 273–281. [CrossRef]
52. Zhang, Z.; Chen, Y.; Wang, P.; Shuai, J.B.; Tao, F.L.; Shi, P.J. River discharge, land use change, and surface water quality in the Xiangjiang River, China. *Hydrol. Process.* **2014**, *28*, 4130–4140. [CrossRef]
53. Daniel, J.L.; Marcello, M.; Paul, E.; Yu, X.Y.; Wei, J.Y.; Li, R.X. Triassic Depositional History of the Yangtze Platform and Great Bank of Guizhou in the Nanpanjiang Basin of South China. *J. Earth Sci. Environ.* **2009**, *31*, 344–367.
54. Fang, X.; Peng, B.; Song, Z.; Wu, S.; Tu, X. Geochemistry of heavy metal−contaminated sediments from the four river inlets of Dongting Lake, China. *Environ. Sci. Pollut. Res.* **2021**, *10*, 1–21. [CrossRef]
55. Wang, L.; Guo, Z.; Xiao, X.; Chen, T.; Liao, X.; Jie, S.; Wu, B. Heavy metal pollution of soils and vegetables in the midstream and downstream of the xiangjiang river, Hunan province. *J. Geogr. Sci.* **2008**, *18*, 353–362. [CrossRef]
56. Jiang, S.; Zhao, H.; Chen, Y.; Tao, Y.; Yang, J.; Ling, H. Trace and rare earth element geochemistry of phosphate nodules from the lower Cambrian black shale sequence in the Mufu Mountain of Nanjing, Jiangsu province, China. *Chem. Geol.* **2007**, *244*, 584–604. [CrossRef]
57. Boynton, W.V. Geochemistry of the rare earth elements: Meteorite studies. *Rare Earth Elem. Geochem.* **1984**, *2*, 63–114.
58. Aide, M.T.; Aide, C. Rare earth elements: Their importance in understanding soilgenesis. *Int. Sch. Res. Not. Soil Sci.* **2012**, *2012*, 1–11.

59. Arthur, M.A.; Sageman, B.B. Marine black shales: Depositional mechanisms and environments of ancient deposits. *Annu. Rev. Earth Planet. Sci.* **1994**, *22*, 499–551. [CrossRef]
60. Hatch, J.R.; Leventhal, J.S. Relationship between inferred redox potential of the depositional environment and geochemistry of the Upper Pennsylvanian (Missourian) Stark Shale Member of the Dennis Limestone, Wabaunsee County, Kansas, USA. *Chem. Geol.* **1992**, *99*, 65–82. [CrossRef]
61. Lerman, A. Lakes: Chemistry, Geology, Physics. *Science* **1979**, *204*, 825–826.
62. Fritz, M.; Unkel, I.; Lenz, J.; Gajewski, K.; Frenzel, P.; Paquette, N.; Lantuit, H.; Körte, L.; Wetterich, S. Regional environmental change versus local signal preservation in Holocene thermokarst lake sediments: Acase study from Herschel Island, Yukon (Canada). *J. Paleolimnol.* **2018**, *60*, 77–96. [CrossRef]
63. Liu, F.; Li, G.; Chen, J. U−Pb ages of zircon grains reveal a proximal dust source of the Xiashu loess, Lower Yangtze River region, China. *Chin. Sci. Bull.* **2014**, *59*, 2391–2395. [CrossRef]
64. Taylor, S.R.; McLennan, S.M. The Continental Crust: Its Composition and Evolution. *J. Geol.* **1985**, *94*, 57–72.
65. Peng, B.; Rate, A.; Song, Z.; Yu, C.; Tang, X.; Xie, S.; Tu, X.; Tan, C. Geochemistry of major and trace elements, and Pb isotopes during weathering of black shales of the lower−Cambrian black shales in central Hunan, China. *Appl. Geochem.* **2014**, *51*, 191–203. [CrossRef]
66. Laveuf, C.; Cornu, S. A review on the potentiality of rare earth elements to tracepedogenetic processes. *Geoderma* **2009**, *154*, 1–12. [CrossRef]
67. Li, X.; Han, Z.; Yang, D.; Chen, Y. REE geochemistry of Xiashu loess in Zhenjiang, Jiangsu Province. *Acta Pedol. Sin.* **2006**, *1*, 1–7.
68. Yang, S.Y.; Jung, H.S.; Choi, M.S.; Li, C.X. The rare earth element compositions of the Changjiang (Yangtze) and Huanghe (Yellow) river sediments. *Earth Planet. Sci. Lett.* **2002**, *201*, 407–419. [CrossRef]
69. Wu, M.; Wen, Q. Rare earth elements in Malan Loess in the middle reaches of the Yellow River. *Chin. Sci. Bull.* **1991**, *36*, 4.
70. Ahmad, I.; Chandra, R. Geochemistry of loess−paleosol sediments of Kashmir Valley, India: Provenance and weathering. *J. Asian Earth Sci.* **2013**, *66*, 73–89. [CrossRef]
71. Alfaro, M.R.; Nascimento, C.W.; Biondi, C.M.; Silva, Y.J.; Accioly, A.M.; Ugarte, A.M.; Estevez, J. Rare−earth−element geochemistry in soils developed in different geological settings of Cuba. *Catena* **2018**, *162*, 317–324. [CrossRef]
72. Xie, Y.; Jie, M.; Guo, L. REE geochemistry of modern eolian dust deposits in Harbin city, Heilongjiang province, China: Implications for provenance. *Catena* **2014**, *23*, 70–78. [CrossRef]
73. Trail, D.; Watson, E.B.; Tailby, N.D. Ce and Eu anomalies in zircon as proxies for the oxidation state of magmas. *Geochim. Cosmochim. Acta* **2012**, *97*, 70–87. [CrossRef]
74. Project Team of Changsha kiln. *Changsha Kiln*; Forbidden City Press: Beijing, China, 1996; pp. 7–28.
75. Wacha, L.; Laag, C.; Grizelj, A.; Tsukamoto, S.; Frechen, M. High−resolution palaeo−environmental reconstruction at Zmajevac (Croatia) over the last three glacial interglacial cycles. *Palaeogeogr. Palaeoclimatol. Palaeoecol.* **2021**, *576*, 110504. [CrossRef]
76. Chandler, D.; Langebroek, P. Southern Ocean sea surface temperature synthesis: Part 2. Penultimate glacial and last interglacial. *Quat. Sci. Rev.* **2021**, *271*, 107190. [CrossRef]
77. Yang, D. The paleoenvironment of the mid−lower regions of Changjiang in the full−glacial period of late pleistocene. *Acta Geogr. Sin.* **1986**, *41*, 302–310.
78. Hao, Q.; Guo, Z.; Qiao, Y.; Bing, X.; Oldfield, F. Geochemical evidence for the provenance of middle Pleistocene loess deposits in southern China. *Quat. Sci. Rev.* **2010**, *29*, 3317–3326. [CrossRef]
79. Perry, C.A.; Hsu, K.J. Geophysical, archaeological, and historical evidence support a solar output model for climate change. *Proc. Natl. Acad. Sci. USA* **2000**, *97*, 12433–12438. [CrossRef] [PubMed]
80. Zhang, X. *Quaternary Environmental Geochemistry in Dongting Lake Area*; Geological Publishing House: Bejing, China, 2007; pp. 256–260.
81. Ge, Q.S.; Zheng, J.Y.; Fang, X.Q.; Man, Z.M.; Zhang, X.Q.; Zhang, P.Y.; Wang, W.C. Winter half−year temperature reconstruction for the middle and lower reaches of the Yellow River and Yangtze River, China, during the past 2000 years. *Holocene* **2003**, *13*, 933–940.
82. Wang, Y.J.; Cheng, H.; Edwards, L.R.; He, Y.Q.; Kong, X.G.; An, Z.S.; Wu, J.Y.; Kelly, M.J.; Dykoski, C.A.; Li, X. The Holocene Asian monsoon: Links to solar changes and North Atlantic climate. *Science* **2005**, *308*, 85–857. [CrossRef]
83. Zhang, H.; Cai, J.F.; Liu, H.P. The palynofloras and climate change in Dajuhu basin of Shennongjia Mountains during the last 12500 a B.P. *J. HuaZhong Norm. Univ. Nat. Sci.* **2002**, *36*, 87–92.
84. Curtis, J.H.; Hodell, D.A.; Mark, B. Climate Variability on the Yucatan Peninsula (Mexico) during the Past 3500 Years, and Implications for Maya Cultural Evolution. *Quat. Res.* **2017**, *46*, 37–47. [CrossRef]
85. Ge, Q.; Hao, Z.; Zheng, J.; Shao, X. Temperature changes over the past 2000 yr in China and comparison with the Northern Hemisphere. *Clim. Past* **2013**, *9*, 1153–1160. [CrossRef]
86. Xu, Z.; Li, T.; Chang, F.; Choi, J.; Lim, D.; Xu, F. Sediment provenance discrimination in northern Okinawa Trough during the last 24 ka and paleoenvironmental implication: Rare earth elements evidence. *J. Rare Earths* **2012**, *30*, 1184–1190. [CrossRef]
87. Yan, S.; Long, Y.; Jiang, C.; Wu, C.; Ling, S. The relationship between the change trend of water level and riverbed evolution in the downstream of Xiangjiang river. *J. Water Resour. Water Eng.* **2019**, *30*, 150–156.
88. Yancheva, G.; Nowaczyk, N.R.; Mingram, J.; Dulski, P.; Haug, G. Influence of the intertropical convergence zone on the East−Asian monsoon. *Nature* **2007**, *445*, 74–77. [CrossRef] [PubMed]

89. Bai, S. Chemo−biostratigraphic Study on the Devonian Frasnian Famennian Event. *Acta Scicentiarum Univ. Pekin.* **1998**, *Z1*, 231–237.
90. Cheng, P. Textual research on the north bank embankment of ancient Jingjiang River. *Hist. Geogr.* **1990**, *8*, 70–76.
91. Li, J.; Wang, S.; Mo, D. Environmental changes and relationships with human activities of Dongtinghu plain since 6000 a BP. *Acta Sci. Nat. Univ. Pekin.* **2011**, *47*, 1041–1048.
92. Singh, P. Geochemistry and provenance of stream sediments of the Ganga River and its major tributaries in the Himalayan region, India. *Chem. Geol.* **2010**, *269*, 220–236. [CrossRef]
93. Li, J.; Sun, C.; Zheng, L.; Yin, X.; Chen, J.; Jiang, F. Geochemical characteristics of rare earth elements in the surface sediments from the Spratly Islands of China. *Mar. Pollut. Bull.* **2017**, *114*, 1103–1109. [CrossRef]
94. Gromet, L.P.; Silver, L.T. Rare earth element distributions among minerals in a granodiorite and their petrogenetic implications. *Geochim. Cosmochim. Acta* **1983**, *47*, 925–939. [CrossRef]
95. Xu, L. *Old Tang Books, Biography of Liu Yan*; Tong Xin Publishing House: Beijing, China, 2012; p. 2934.
96. Caggianelli, A.; Fiore, S.; Mongelli, G.; Salveminic, A. REE distribution in the clay fraction of pelites from the southern Apennines, Italy. *Chem. Geol.* **1992**, *99*, 253–263. [CrossRef]
97. Yang, S.Y.; Wang, Z.B. Rare Earth Element Compositions of the Sediments from the Major Tributaries and the Main Stream of the Changjiang River. Bulletin of Mineralogy. *Petrol. Geochem.* **2011**, *30*, 31–39.
98. Gao, A.G.; Chen, Z.H.; Liu, Y.G. Geochemical characteristics of rare earth elements in the surface sediments of Chukchi Sea. *Sci. China Ser. D* **2003**, *33*, 148–157.
99. Dou, Y.G.; Li, J.; Li, Y. Rare earth element compositions and provenance implication of surface sediments in the eastern Beibu Gulf. *Geochimica* **2012**, *41*, 147–157.
100. Condie, K.C. Geochemical changes in basalts and andesites across the Archean−Proterozoic boundary: Identification and significance. *Lithos* **1989**, *23*, 1–18. [CrossRef]
101. Wang, X.; Lu, H.; Zhang, H.; Wu, J.; Hou, X.; Fu, Y.; Geng, J. Distribution, provenance, and onset of the Xiashu Loess in Southeast China with paleoclimatic implications. *J. Asian Earth Sci.* **2017**, *155*, 180–187. [CrossRef]
102. Ye, H.; Wu, C.Z.; Yang, T.; Santosh, M.; Yao, X.Z.; Gao, B.F.; Wang, X.L.; Li, W. Updating the Geologic Barcodes for South China: Discovery of Late Archean Banded Iron Formations in the Yangtze Craton. *Sci. Rep.* **2017**, *7*, 15082. [CrossRef]
103. Wei, X.; Wen, X.F.; Yang, R.D. Trace element distribution characteristics and correlation analysis of modern weathering crust profile of Neoproterozoic Epimetamorphic rocks in Darong, Congjiang County, Guizhou province. *Earth Environ.* **2010**, *38*, 304–313.
104. Chen, W.F.; Chen, P.R.; Huang, H.Y.; Ding, X.; Sun, T. Chronological and geochemical studies of granite and enclave in Baimashan pluton, Hunan, South China. *Sci. China Ser. D Earth Sci.* **2007**, *37*, 873–893. [CrossRef]
105. Chen, H.; Chen, Z.; Chen, Z.; Ma, Q.; Zhang, Q. Rare earth elements in paddy fields from eroded granite hilly land in a southern China watershed. *PLoS ONE* **2019**, *14*, e0222330. [CrossRef]
106. Guo, A.; Mao, L.; Zhang, X.; Mo, D.; Zou, C.; Li, Y.; Wu, Y. An analysis of the factors influencing the rise and fall of Changsha kiln in Tang Dynasty. *Cult. Relics South. China* **2020**, *5*, 146–154.